Diagnosis of Relative Humidity Changes in a Warmer Climate Using Tracers of Last Saturation

Jonathon S. Wright * and Adam Sobel

Department of Applied Physics and Applied Mathematics, Columbia University, New York, NY USA

Joseph Galewsky

Department of Earth and Planetary Sciences, University of New Mexico, Albuquerque, NM USA

* *Corresponding author address:* Jonathon Wright, Columbia University, Department of Applied Physics and Applied Mathematics, 500 West 120th St, New York, NY 10027 USA.

E-mail: jw2519@columbia.edu

ABSTRACT

The zonal mean relative humidity response to a doubling of CO_2 in a climate model is examined, using two different methods to differentiate the effects of circulation changes from spatially inhomogeneous temperature changes. The tropical and subtropical response are found to be largely dependent on circulation changes, particularly a poleward expansion and deepening of the Hadley circulation, a poleward shift of the extratropical jets, and an increase in the height of the tropopause. The responses near the extratropical tropopause and in the lower troposphere are largely dependent on changes in the distribution and gradients of temperature.

1. Introduction

Climate models indicate that the water vapor feedback is roughly equivalent to that expected from constant global mean relative humidity (RH) (Soden and Held 2006; Randall et al. 2007). Analyses of observed climate variations in the recent historical record are consistent with this view (Soden et al. 2002; Dessler et al. 2008). A constant global mean RH does not necessarily correspond to a static distribution of RH, however, and even small changes can be consequential for other aspects of the climate (e.g., Sherwood et al. 2009).

Relative humidity is an important factor in determining the distribution and occurrence of clouds (Sundqvist 1978; Price and Wood 2002). An increase in the fraction of optically thin high clouds with warming would represent a positive feedback, as such clouds are relatively transmissive to sunlight, largely opaque to outgoing longwave radiation, and have a substantially different emission temperature than the surface. The converse is true for low clouds, as the increase in solar albedo that they provide outweighs their effect as longwave absorbers (Manabe and Strickler 1964; Hartmann et al. 1992; Chen et al. 2000). A greater understanding of the underlying causes of simulated RH changes and their plausibility may therefore be helpful in constraining cloud feedbacks, which currently represent the largest source of inter-model spread in climate sensitivity (Randall et al. 2007). Inhomogeneity in RH changes also impacts the distribution of both latent and radiative heating, which may then project onto the atmospheric circulation (Schneider et al. 2009), large-scale convective organization (Gray and Jacobson 1977), and the level at which deep convection detrains (Hartmann and Larson 2002). Regional shifts of the climatological distribution of RH thus have the potential to influence climate on a wide range of scales.

Several studies have noted that the simulated RH response to warming exhibits a distinctive zonal mean pattern (Mitchell and Ingram 1992; Lorenz and DeWeaver 2007a; Sherwood et al. 2009). This pattern is characterized by a horseshoe-shaped decrease of relative humidity throughout the tropical upper troposphere, subtropics, and extratropical free troposphere, with a slightly more pronounced decrease in the southern hemisphere. This horseshoe is bracketed by an increase of relative humidity in the tropical mid-troposphere and extratropical tropopause layer, as shown in Fig. 1. The RH difference shown in Fig. 1 is averaged over ten models in the World Climate Research Program's (WCRP's) Coupled Model Intercomparison Project phase 3 (CMIP3) multi-model dataset, and is calculated using time mean zonal mean relative humidities from the final five years of the slab ocean control (SlabCNTL) and doubled carbon dioxide (2xCO2) experiments. Although the details of the signal vary among constituent models, the qualitative pattern is largely robust.

Relative humidity is defined in this analysis as the ratio of specific humidity to saturation specific humidity. Saturation specific humidity is a function of local temperature as expressed by the Clausius-Clapeyron equation. Free tropospheric specific humidity is in turn determined to leading order by the large-scale circulation and temperature fields, with condensate evaporation playing a minor role (Sherwood 1996; Pierrehumbert and Roca 1998; Galewsky et al. 2005; Sherwood and Meyer 2006; Wright et al. 2009b).

Unsaturated air parcels conserve specific humidity. To the extent that condensate evaporation is unimportant, the specific humidity in unsaturated air equals the saturation specific humidity at the point at which it was last saturated. Galewsky et al. (2005, hereafter GSH) used "tracers of last saturation" to trace the pathways taken by air parcels since their points of last saturation. This technique provides insight into the ways in which the circulation and temperature fields together determine the distributions of atmospheric specific and relative humidity. Here we apply an updated formulation of this tracer technique to the output of two integrations of a GCM, one of which simulates modern climate and one of which simulates a climate with doubled CO_2. The results help to establish the relative influences of shifts in atmospheric circulation as compared to inhomogeneous changes in temperature on the characteristic RH response shown in Fig. 1.

2. Model Configuration

This study employs a two-level global modeling procedure to investigate the mechanisms behind relative humidity change in a warmer climate. First, a GCM is run to provide six-hourly circulation and temperature fields that are representative of both a modern (CTL) and doubled CO_2 (WRM) climate. These meteorology fields are then used as inputs to a global tracer transport model, which includes an independent hydrologic cycle and is outfitted with a last saturation tracer scheme (GSH; Hurley and Galewsky 2009).

a. General Circulation Model

The base meteorology for this study is generated by two integrations of the Goddard Institute for Space Studies (GISS) ModelE (Schmidt et al. 2006). The first of these, designated CTL, uses atmosphere and ocean conditions consistent with the year 1979, including greenhouse gas concentrations and sea surface temperatures. The second simulation is designated WRM, and is performed using a slab ocean version of the model with atmospheric CO_2

doubled from the 1979 value at the outset. The concentration of atmospheric CO_2 is held constant at 337.1 ppmv for the CTL simulation and 674.2 ppmv for the WRM simulation.

Both model simulations are run at $2°$ latitude by $2.5°$ longitude resolution with 20 vertical levels. Advection of temperature and water vapor conserves potential enthalpy and mass, and is computed using a quadratic upstream scheme with nine higher-order moments (Prather 1986). This yields an effective tracer resolution of approximately $0.7°\times0.8°$. The model physics and radiation are described in detail by Schmidt et al. (2006).

Sea surface temperatures and sea ice extent for the CTL simulation follow a fixed annual cycle averaged over 1975 to 1984, with all other boundary conditions set to 1979 values as discussed by Schmidt et al. (2006). Atmospheric CO_2 is also kept constant at 1979 levels. This simulation is run for ten years; output from the last five years is used for this analysis.

The WRM simulation is similar to the CTL simulation, with the addition of a mixed layer heat flux model (q-flux) and doubled CO_2. Initial mixed layer heat transport is prescribed using implied values from a five-year climatology generated during the CTL simulation. Net global heating at the surface during the CTL run is $0.09\,\mathrm{W\,m^{-2}}$, well within the $\pm0.5\,\mathrm{W\,m^{-2}}$ threshold recommended for a q-flux setup run (Schmidt et al. 2006). The mixed layer depth varies according to a fixed seasonal cycle and is assumed to be isothermal. Energy is conserved by incorporating fluxes between the mixed layer and a deeper layer between the base of the current mixed layer and the base of the mixed layer at its annual maximum depth. Sea surface temperatures and sea ice extent are determined dynamically during the model integration.

Instantaneous meteorological variables are saved every six hours during each model run. Saved surface variables include orography, surface geopotential, surface temperature, surface pressure, latent heat flux, sensible heat flux, and the zonal and meridional components of surface stress. Atmospheric variables are saved at all 20 vertical levels and include temperature, specific humidity, and zonal and meridional winds. For compatibility with the tracer transport model, these data are interpolated from the ModelE's $2° \times 2.5°$ latitude-longitude grid to a T42 Gaussian grid using bilinear interpolation. The vertical coordinate is unchanged.

b. Tracer Transport Model

Tracer transport is accomplished using the offline Model for Atmospheric Transport and Chemistry (MATCH) developed at the National Center for Atmospheric Research (NCAR) (Rasch et al. 1997). The MATCH model uses a semi-Lagrangian advection scheme, and includes an independent hydrologic cycle with parameterizations for cloud physics and convection.

The MATCH integrations presented here are performed using a 30 minute timestep, with linear interpolation between the six-hourly meteorological fields. The model is run on a T42 Gaussian horizontal grid with 20 hybrid sigma vertical levels, matching the input meteorological data. Tracer advection is calculated using a semi-Lagrangian transport scheme with enforced mass conservation (Rasch and Williamson 1990; Rasch et al. 1995). Subgrid-scale turbulent mixing is represented by a vertical eddy diffusion parameterization.

The parameterizations for clouds and convection are based on those developed for version 3 of the NCAR Community Climate Model (CCM3). In particular, MATCH uses the prognostic cloud parameterization presented by Rasch and Kristjansson (1998) and the convection scheme described by Hack et al. (1998). The convective parameterization partitions convective transport into deep convection (Zhang and McFarlane 1995) and shallow convection (Hack 1994). Tracers are advected both within the convective paramaterization and by the large-scale circulation.

c. *Tracer Formulation*

The base formulation of the tracers of last saturation follows that of GSH. Specifically, a set of N zonally symmetric tracer domains is chosen to cover the global troposphere. Each grid point is associated with the domain that contains it; we will call the tracer associated with this domain the local tracer ($\mathcal{L}$) and all others nonlocal tracers ($\mathcal{T}_i$; $i = 1, \cdots, N-1$).

All tracers are initially set to zero. During model integration, whenever free tropospheric RH exceeds a saturation threshold of 90% the local tracer is set to one and all nonlocal tracers are set to zero at that point:

$$\begin{aligned}
\mathcal{L}(\lambda, \phi, p, t) &= 1 \\
\mathcal{T}_i(\lambda, \phi, p, t) &= 0|_{i=1,\cdots,N-1} \\
\mathcal{S}(\lambda, \phi, p, t) &= 0 \\
\mathcal{S}_{\mathrm{amt}}(\lambda, \phi, p, t) &= 0,
\end{aligned}$$

where λ and ϕ represent the longitude and latitude of the saturated grid cell, p represents the vertical coordinate, and t denotes the model timestep. $\mathcal{S}$ and $\mathcal{S}_{\mathrm{amt}}$ are the surface source tracers, which are defined below. Whenever the local RH is below the threshold value, the tracers of last saturation are permitted to advect and mix unchanged. A RH threshold of

90% is chosen to reflect the fact that saturation operates at spatial scales well below the grid scale; that is, some air parcel in the grid volume may be at saturation even though the mean RH for the entire volume is below 100%. The results are insensitive within reasonable perturbations to this threshold (±10% RH). Saturation is determined according to MATCH's internal hydrologic cycle, rather than the GCM output.

The evaporative source at the surface is incorporated by treating the lowest model layer separately: all last saturation tracers in this layer are set to zero and a source tracer ($\mathcal{S}$) is defined with a value equal to the current specific humidity (q) in the grid cell:

$$
\begin{aligned}
\mathcal{T}_i(\lambda, \phi, p_b, t) &= 0|_{i=1,\cdots,N} \\
\mathcal{S}(\lambda, \phi, p_b, t) &= q(\lambda, \phi, p_b, t) \\
\mathcal{S}_{\mathrm{amt}}(\lambda, \phi, p_b, t) &= 1,
\end{aligned}
$$

p_b denotes the lowest model layer. Note that the local tracer $\mathcal{L}$ is replaced by $\mathcal{S}$ at the surface, so that there are N nonlocal tracers rather than $N-1$. For bookkeeping purposes we also define a source amount tracer $\mathcal{S}_{\mathrm{amt}}$ that follows the definitions of $\mathcal{L}$ and $\mathcal{T}$. The source tracer is permitted to mix, so that the value of $\mathcal{S}$ at any location may reflect several excursions to the surface.

The local specific humidity $q(\lambda, \phi, p, t)$ can then be reconstructed via the linear combination

$$
q(\lambda, \phi, p, t) = \mathcal{L}(\lambda, \phi, p, t) q^*(\lambda, \phi, p, t) + \sum_i^{N-1} \mathcal{T}_i(\lambda, \phi, p, t) \langle q_i^* \rangle + \mathcal{S}(\phi, p) \qquad (1)
$$

where $q^*(\lambda, \phi, p, t)$ is the local saturation mixing ratio and $\langle q_i^* \rangle$ represents the density weighted mean saturation specific humidity for tracer domain i. The tracers generally obey the constraint

$$\mathcal{L}(\lambda, \phi, p, t) + \sum_{i}^{N-1} \mathcal{T}_i(\lambda, \phi, p, t) + \mathcal{S}_{\text{amt}}(\lambda, \phi, p, t) = 1 \tag{2}$$

in our simulations; after a brief initial spin-up period significant deviations from the occur only in the stratosphere. RH is then reconstructed as

$$\text{RH}(\lambda, \phi, p, t) = \frac{q(\lambda, \phi, p, t)}{q^*(\lambda, \phi, p, t)} \tag{3}$$

with $q(\lambda, \phi, p, t)$ determined by Eq. 1. GSH discuss technical issues involved in this reconstruction and quantify several sources of error.

Figure 2 shows a direct comparison between the modeled and reconstructed zonal mean RH fields for the MATCH integration using CTL meteorological fields as input. The qualitative patterns match up remarkably well, and the point to point comparison also indicates excellent agreement in both the tropics and extratropics. Excluding the model layers below 900 hPa and above 110 hPa, where boundary layer or stratospheric influences render the reconstruction less effective, the Pearson correlation coefficients between modeled and reconstructed RH are greater than 0.95.

Figure 2 includes two adjustments to the tracer scheme presented by GSH. First, we have altered the distribution of tracer domains (defined by dotted black lines). Although the chosen domains remain zonally axisymmetric, they now provide global coverage (as opposed to 50°S to 50°N in GSH). The horizontal resolution of the tracer domains is approximately 5° latitude equatorward of 50°, with a ∼15° domain out to 65° and a 25° domain extending to the pole in both hemispheres. We also increase the tracer domain resolution with altitude, so that the vertical domain sizes are roughly equivalent in $\log(p)$ space. This allows us to better diagnose the mechanisms influencing upper tropospheric humidity, particularly in the tropics. Second, we have applied a temperature correction to the online tracer calculation. The GSH formulation predicted extremely high humidities in the upper troposphere. This bias resulted from the transport of trace amounts of source and lower tropospheric tracer into the upper troposphere. Although these tracer concentrations were quite small, they were associated with values of $\langle q^* \rangle$ that were comparatively quite high, and thus exerted a disproportionately large influence on the reconstructed humidity. We have addressed this issue by including an online calculation of density weighted mean temperature $\langle T_i \rangle$ for each tracer domain. At each timestep, if $\langle T_i \rangle > T(\lambda, \phi, p)$, then that tracer is converted to local tracer:

$$\mathcal{L}(\lambda, \phi, p) = \mathcal{L}(\lambda, \phi, p) + \mathcal{T}_i(\lambda, \phi, p)$$

$$\mathcal{T}_i(\lambda, \phi, p) = 0|_{\langle T_i \rangle > T(\lambda, \phi, p)}.$$

This adjustment compensates for any spurious vertical tracer transport that does not lead to grid scale saturation, and is physically equivalent to assuming that condensate is immediately removed at the subgrid scale in both parameterized convective updrafts and vertical advection.

3. Simulated Climate Changes

Investigation of the mechanisms underlying the characteristic pattern shown in the multimodel mean RH changes (Fig. 1) requires meteorological output from a GCM that exhibits this pattern of change as climate warms. Figure 3 shows the RH difference between the WRM and CTL runs of the GISS ModelE. The changes between these two runs agrees quite well with the multimodel mean change, both qualitatively and quantitatively. This indicates that the ModelE is a reasonable choice for examining the root causes behind the pattern of RH changes.

A number of studies have examined the distribution of circulation and temperature changes in the model simulations submitted to the CMIP3 intercomparison project (e.g., Randall et al. 2007; Lorenz and DeWeaver 2007b; Vecchi and Soden 2007; Lu et al. 2008; Gastineau et al. 2008). In general, these studies find that the tropopause height increases, the tropical overturning circulation expands poleward, deepens, and weakens, the subtropical jets shift poleward, the lapse rate of temperature with altitude is reduced, and the equator-to-pole temperature gradient in the upper troposphere is increased. These findings are generally supported by observational studies that focus on recent trends in atmospheric temperature and circulation (e.g., Santer et al. 2003; Seidel and Randel 2006; Hu and Fu 2007), although there is some disagreement with observed trends in the strength of the Hadley cell (Mitas and Clement 2006).

Figure 4 shows simulated circulation and temperature changes between the CTL and WRM runs of the ModelE GCM. The troposphere warms nearly everywhere (Fig. 4a; shading), with the strongest warming in the tropical upper troposphere. This reduces the tropospheric lapse rate in the tropics and subtropics. The equator-to-pole temperature gradient is reduced in the lower troposphere and increased in the upper troposphere. Changes in zonal mean streamfunction (Fig. 4a; black contours) indicate that the Hadley cell expands and deepens. Taken together with the warming in the tropical upper troposphere, the latter is at least qualitatively consistent with the fixed anvil temperature hypothesis, which postulates that tropical convective detrainment is constrained to occur at roughly the same temperature as climate changes (Hartmann and Larson 2002). The strength of the Hadley circulation is very similar between the CTL and WRM slab ocean simulations of the ModelE, with a slight strengthening or weakening depending on the metric used. Vecchi and Soden (2007) and others report that the tropical overturning circulation weakens in the CMIP3 models; however, this decrease is primarily manifested in the Walker circulation rather than the Hadley cell. The strength of the longitudinal Walker circulation in the ModelE decreases in WRM simulation (not shown), consistent with this consensus. Gastineau et al. (2008) show that changes in the strength of the Hadley cell are much more variable in CMIP3 models, and Mitas and Clement (2006) report recent positive trends in reanalysis data that are not reproduced by GCM simulations of twentieth century climate. In the context of current scientific understanding, the representation of changes in the strength of the tropical overturning circulation is reasonable and consistent with expectations.

Shifts in the zonal mean zonal wind (Fig. 4a; white contours) indicate that the subtropical jets intensify and shift poleward in the ModelE, consistent with the CMIP3 multimodel mean (Lorenz and DeWeaver 2007b). Figure 4b shows zonal mean tropopause height and temperature changes for the World Meteorological Organization (WMO; 1957) tropopause. Tropopause pressure (height) decreases (increases) globally with a minimum shift in the tropics, while tropopause temperature increases everywhere but in the deep tropics, which exhibit a slight cooling. Both of these are consistent with the the CMIP3 multimodel means (Lorenz and DeWeaver 2007b) and with observations of recent anthropogenic trends (Santer et al. 2003).

If the multimodel means and existing observational studies are considered as a baseline consensus, the circulation and temperature changes simulated by the GISS ModelE are generally consistent with this consensus. One important caveat is that ozone levels in the simulations presented here are fixed at 1979 values, so the impacts of stratospheric ozone recovery on circulation and humidity changes (Son et al. 2008, 2009) are not included in this analysis.

4. Tracer Model Experiments

The GCM simulations provide a means by which to describe the control and doubled CO_2 climates. The MATCH tracer transport model is employed at the second level because it affords greater flexibility. By separating calculations of the tracer distribution from the circulation and temperature fields that determine them, the mechanisms that control the distribution of RH changes can be better identified and isolated. It is therefore important that the results of the MATCH runs using GISS output are similarly able to reproduce the expected pattern of RH change. Figure 5 shows the zonal mean difference of RH between the WRM and CTL runs for the MATCH model hydrologic cycle. The contents of this figure closely mirror those of Fig. 3.

The MATCH runs are forced using ModelE output. This leaves two significant differences between the simulations used to prepare Fig. 3 and those used to prepare Fig. 5: the advection scheme and the hydrologic cycle parameterizations. The close correspondence between the pattern of RH change in MATCH and that in the GCM suggests that the distribution of RH changes is not strongly sensitive to the details of these two parameterizations. This conclusion is supported by the robust nature of the pattern among the CMIP3 model simulations, which also contain a variety of advection and microphysical parameterizations. We note, however, that the MATCH model and most of the CMIP3 models indicate a stronger RH signal throughout the troposphere than the ModelE. Humidity in the ModelE exhibits a fairly strong dependence on condensate evaporation (Wright et al. 2009b), together with much higher ice water paths than either observations or other GCMs (Waliser et al. 2009). The occurrence of condensate evaporation is strongly dependent on ambient RH: less condensate evaporates at higher RH while more condensate evaporates at lower RH (Dessler and Sherwood 2004; Wright et al. 2009a). It is not possible to differentiate the signals sufficiently to draw firm conclusions, but the evidence suggests that the weaker signal in the ModelE may be attributed to a greater role of condensate evaporation in that GCM. It follows then that if condensate evaporation exerts a larger influence on humidity than is currently believed then the strength of the RH signal shown in Fig. 1 will be suppressed. This would nudge the climate closer to true constant RH, likely leading to a slight increase the strength of the water vapor feedback (Soden et al. 2002; Minschwaner and Dessler 2004; Minschwaner et al. 2006).

Relative humidity at any given point will remain constant under climate change so long as the saturation mixing ratio changes by the same fraction at the point in question and at the relevant point(s) of last saturation. Loosely speaking, this would occur over the entire atmosphere if the circulation remains relatively constant and the temperature changes are spatially uniform. On the other hand, the circulation does change and temperature changes have spatial structure in climate model simulations of warming (e.g., Randall et al. 2007; Lorenz and DeWeaver 2007b; Lu et al. 2008). We wish to attribute the changes in RH shown in Fig. 1 to these two factors. To what extent are these changes driven by circulation shifts, and to what extent are they driven by spatially inhomogeneous temperature changes?

As a brute force method of separating the roles of circulation and temperature, we run the MATCH model with temperature and circulation fields chosen from different GCM simulations. MATCH is run with WRM temperatures and CTL circulation and vice versa. This is dynamically inconsistent, since temperature and winds are related through the equations of motion. On the other hand, it is kinematically acceptable for the purpose of diagnosing the mechanisms controlling water vapor; the water vapor simply evolves in space and time according to a given set of temperature and wind fields. This approach leverages the offline tracer transport to separate temperature and circulation in a way that could not be done in a dynamically consistent calculation.

Figure 6a shows RH changes between the CTL MATCH simulation and a simulation in which WRM atmospheric temperatures are combined with the CTL circulation. This difference does not show the characteristic horseshoe-shaped pattern of RH decrease throughout the troposphere, particularly in the tropical and subtropical upper troposphere. It does capture the RH increases near the extratropical tropopause and in the lower stratosphere, however, and many aspects of the lower tropospheric response. Figure 6b shows the same quantity for a MATCH simulation in which the WRM circulation is combined with CTL atmospheric temperatures. In this case, the tropical and subtropical free tropospheric response is captured quite well, although the RH decrease near the extratropical tropopause does not appear. Figure 6 thus indicates that RH changes in the tropical and subtropical troposphere are dominated by circulation changes, whereas the increase near the extratropical tropopause and changes in near-surface RH are controlled by temperature changes.

The high latitude tropospheric response is far too strong in both perturbation simulations; in fact, Fig. 3 and Fig. 5 indicate that changes in these regions should be small and of variable sign, rather than the strongly negative response shown in both panels of Fig. 6. This mismatch may be a consequence of the shallow convective parameterization in MATCH, which can moisten the troposphere without causing grid-scale saturation and which is not handled explicitly by our tracer technique. It could also simply be a result of nonlinearities: tracer transport is linear, but saturation is nonlinear. Thus, the results in Figs. 6a and 6b need not add up to those in Fig. 5 in general, although they do so (approximately) in the tropics and subtropics, and at the extratropical tropopause.

5. Last Saturation Tracers

Figure 2 indicates that the tracer reconstruction of RH agrees both qualitatively and quantitatively with the RH simulated by MATCH using CTL meteorology. This agreement translates to RH changes between the CTL and WRM runs, as shown in Fig. 7. The reconstruction captures much of the structure observed in both the GISS model (Fig. 3) and the online MATCH hydrologic cycle (Fig. 5), in particular the horseshoe-shaped RH decrease and the increases in the tropical middle troposphere and extratropical tropopause layer. The tracer reconstruction of RH does not capture the increase of RH in the lower stratosphere, but this is unsurprising since our choice of tracer domains effectively omits the stratosphere.

This agreement provides a check on the consistency of the tracer formulation. Since the RH reconstruction successfully captures the pattern of RH changes in the warmer climate, the tracers can be applied to diagnose some of the relevant mechanisms.

A simple diagnostic that can be constructed from the last saturation tracers invloves separating contribution of changes in the local tracer $\mathcal{L}(\lambda, \phi, p)$, which represents the amount of air in a grid cell (λ, ϕ, p) that was last saturated with the tracer domain containing that cell, from that of all nonlocal tracers $\sum_i^{N-1} \mathcal{T}_i(\lambda, \phi, p)$. Although it only makes use of a small fraction of the information carried by the tracers, this diagnostic appears to explain a large portion of the RH change. Figure 8 shows the zonal and time mean change in the concentration of $\mathcal{L}$. The pattern of changes in $\mathcal{L}$ agrees remarkably well with the pattern of changes in simulated RH. In particular, if the proportion of air that is last saturated locally decreases then the RH tends to decrease, and vice versa. This correspondence is expected, as air that was last saturated nearby is likely to be closer to saturation now.

The close correspondence between the pattern of changes in RH and the pattern of changes in $\mathcal{L}$ is particularly relevant near the extratropical tropopause in both hemispheres. These regions experience an increase in the concentration of local tracer $\mathcal{L}$, which acts to increase RH by increasing the contribution of $q^*(\phi, p)$ to $q(\phi, p)$ (Eqn. 1). This is driven in large part by the gradient of temperature changes in the upper troposphere. In the CTL simulation, humidity near the extratropical tropopause is determined to a significant extent by equatorward zones of last saturation. The greatest warming occurs in the tropical upper troposphere, with diminished warming toward the poles (Fig. 4). This gradient of warming acts to increase the local control of humidity near the extratropical and polar tropopause; this increase of local control results in an increase of RH. The increase of RH in this region may in turn lead to an increase in the occurrence of high thin clouds near the extratropical tropopause, with implications for cloud radiative forcing. Examination of the GCM results indicates that total cloud cover increases in these regions by 1% to 5% (not shown), due to an increase in the occurrence of cirrus ice clouds that are formed in situ.

As with the MATCH perturbation simulations presented in Section 4, the tracer reconstruction of RH (Eqs. 1 and 3) can be broken down into two components: one representing the circulation (the tracers), and one representing temperatures (q^*) (cf. Hurley and Galewsky 2009). This attribution is not clean, because the temperature field influences the tracers as well; if the circulation were held fixed, changes in temperature would change the locations at which saturation occurs, thus changing the tracer fields. Nonetheless, the correspondence of many aspects of the results below with those in the previous section — in which an entirely different method with different limitations was used to separate the roles of temperature and circulation — suggests that there is some validity to the conclusions.

Figure 9 shows zonal mean changes in reconstructed RH using WRM calculations of q^* with CTL tracers (Fig. 9a), and WRM tracers with CTL q^* (Fig. 9b).

These results support the conclusions drawn from Fig. 6. In particular, circulation changes appear to play a dominant role in RH changes in the tropical troposphere, while inhomogeneous changes in temperature appear to control the RH increase near the extratropical tropopause. These responses can be illustrated in further detail using the last saturation tracer distributions.

Figure 10 shows changes in the concentration of two sets of tracers in the tropical upper troposphere. The first set (left panels) is associated with the layer between 288 hPa and 212 hPa, while the second set (right panels) is associated with the layer above (212 hPa to 150 hPa). There is a dramatic transfer of influence from the lower level to the upper one; the concentration of the lower set of tracers decreases throughout the tropical troposphere and appears to be largely replace by tracer from the upper set. This transfer represents an upward shift in the zones of last saturation throughout the tropics, consistent with an upward shift in the tropopause as shown in Fig. 4b, and as expected from the fixed anvil temperature hypothesis (Hartmann and Larson 2002).

Figure 11 shows changes in tracer concentrations associated with humidity in the subtropical free troposphere. This figure shows that the primary regions of last saturation for the subtropical dry zones shift upward and poleward in the warmer climate. These changes are consistent with an expansion of the tropical Hadley cell and a poleward shift in the jetstreams, as shown in Figure 4. In particular, both circulation and tracer shifts are more pronounced in the southern hemisphere. The decrease of RH in the southern hemisphere is also stronger in the ModelE, MATCH, tracer reconstruction, and CMIP3 multimodel mean. As mentioned above, these model runs do not include stratospheric ozone recovery, so these asymmetries are likely due to differences in the distribution of the continents and orography between the northern and southern hemispheres.

6. Summary

The zonal mean signature of the relative humidity response to a doubling of CO_2 is qualitatively robust across climate models. This signature is characterized by a horseshoe-shaped decrease of relative humidity in the tropical upper troposphere, subtropics, and extratropical free troposphere, with a stronger decrease in the southern hemisphere, and an increase of RH in the tropical mid-troposphere and extratropical tropopause layer.

Two climate model simulations are performed, one of modern climate and one with doubled CO_2. Humidity and circulation changes between these simulations are generally representative of the model simulations submitted to the CMIP3 model intercomparison project. Six-hourly meteorological output from the GCM simulations is used to drive a three-dimensional offline tracer transport model that contains both an independent hydrologic cycle and a zonally axisymmetric last saturation tracer scheme. The tracers are capable of quantitatively and qualitatively capturing both the modeled RH field and the pattern of RH response to warming. Two different methods are then used to separate the role of circulation from that of temperature.

Two perturbation simulations are performed using the tracer transport model that pair modern circulation with doubled CO_2 temperatures and vice versa. The results of these simulations indicate that the horseshoe-shaped pattern of RH decrease is driven primarily by circulation shifts, particularly in the tropical and subtropical upper troposphere, while RH increases near the extratropical tropopause and changes near the surface appear to be controlled by inhomogeneities in the temperature response to a doubling of CO_2. Similar conclusions are reached by manipulating the tracer reconstruction of RH to better differentiate between the contributions of circulation, local temperature, and nonlocal temperatures.

Much of the zonal mean RH response is captured by the binary distinction between local and nonlocal last saturation tracers; that is, if the amount of air in a grid cell that was last saturated nearby increases, the RH generally increases as well, and vice versa. This correspondence is particularly relevant near the extratropical tropopause, which exhibits an increase in RH that is associated primarily with an increase in local last saturation. Both of these are driven in large part by the gradient of temperature changes in the upper troposphere and at the tropopause, and lead to an increase in high clouds with substantial implications for cloud radiative forcing in the extratropics and polar regions.

The last saturation tracers are used to illustrate the influence of simulated circulation shifts on zonal mean RH. In particular, last saturation zones for the tropical upper troposphere shift upward in the doubled CO_2 climate, resulting in a RH decrease. This shift is consistent with the upward shift of the tropopause and the deepening of tropical convection associated with the Hadley Cell observed in the simulation. Similarly, the tracers of last saturation that control RH in the subtropical dry zones shift upward and poleward in the warmer climate, consistent with a poleward expansion of the tropical circulation and a poleward shift of the extratropical jets.

Acknowledgments.

We thank Gavin Schmidt and Tony Del Genio for assistance with the ModelE. We also acknowledge the modeling groups for making their model output available for analysis, the Program for Climate Model Diagnosis and Intercomparison (PCMDI) for collecting and archiving this data, and the WCRP's Working Group on Coupled Modelling (WGCM) for organizing the model data analysis activity. The WCRP CMIP3 multi-model dataset is supported by the Office of Science, U.S. Department of Energy. This work was supported by NASA grant number NNX06AB01G and NSF grant number ATM-0542736.

REFERENCES

Chen, T., W. B. Rossow, and Y. Zhang, 2000: Radiative effects of cloud-type variations. *J. Clim.*, **13**, 264–286.

Dessler, A. E. and S. C. Sherwood, 2004: Effect of convection on the summertime extratropical lower stratosphere. *J. Geophys. Res.*, **109**, D23301, doi:10.1029/2004JD005209.

Dessler, A. E., Z. Zhang, and P. Yang, 2008: Water-vapor climate feedback inferred from climate fluctuations, 2003-2008. *Geophys. Res. Lett.*, **35**, L20704, doi:10.1029/2008GL035333.

Galewsky, J., A. Sobel, and I. Held, 2005: Diagnosis of subtropical humidity dynamics using tracers of last simulation. *J. Atmos. Sci.*, **62**, 3353–3367.

Gastineau, G., H. Le Treut, and L. Li, 2008: Hadley circulation changes under global warming conditions indicated by coupled climate models. *Tellus A*, **60A**, 863–884.

Gray, W. M. and R. W. Jacobson, 1977: Diurnal variation of deep cumulus convection. *Mon. Wea. Rev.*, **105**, 1171–1188.

Hack, J., 1994: Parameterization of moist convection in the NCAR Community Climate Model, CCM2. *J. Geophys. Res.*, **99**, 5551–5568.

Hack, J., J. Kiehl, and J. Hurrell, 1998: The hydrologic and thermodynamic characteristics of the NCAR CCM3. *J. Clim.*, **11**, 1179–1206.

Hartmann, D. L. and K. Larson, 2002: An important constraint on tropical cloud-climate feedbacks. *Geophys. Res. Lett.*, **29**, doi:10.1029/2002GL015835.

Hartmann, D. L., M. E. Ockert-Bell, and M. L. Michelsen, 1992: The effect of cloud type on Earth's energy balance: Global analysis. *J. Clim.*, **5**, 1281–1304.

Hu, Y. and Q. Fu, 2007: Observed poleward expansion of the Hadley circulation since 1979. *Atm. Chem. Phys.*, **7**, 5229–5236.

Hurley, J. V. and J. Galewsky, 2009: A last-saturation analysis of ENSO humidity variability in the subtropical Pacific. *J. Clim.*, in press.

Lorenz, D. J. and E. T. DeWeaver, 2007a: The response of the extratropical hydrological cycle to global warming. *J. Clim.*, **20**, 3470–3484.

Lorenz, D. J. and E. T. DeWeaver, 2007b: Tropopause height and zonal wind response to global warming in the IPCC scenario integrations. *J. Geophys. Res.*, **112**, D10119, doi:10.1029/2006JD008087.

Lu, J., G. Chen, and D. W. Frierson, 2008: Response of the zonal mean atmospheric circulation to El Niño versus global warming. *J. Clim.*, **21**, 5835–5851.

Manabe, S. and R. F. Strickler, 1964: Thermal equilibrium of the atmosphere with a convective adjustment. *J. Atm. Sci.*, **21**, 361–385.

Minschwaner, K. and A. E. Dessler, 2004: Water vapor feedback in the tropical upper troposphere: Model results and observations. *J. Clim.*, **17**, 1272–1282.

Minschwaner, K., A. E. Dessler, and P. Sawaengphokhai, 2006: Multimodel analysis of the water vapor feedback in the tropical upper troposphere. *J. Clim.*, **19**, 5455–5464.

Mitas, C. M. and A. Clement, 2006: Recent behavior of the Hadley cell and tropical thermodynamics in climate models and reanalyses. *Geophys. Res. Lett.*, **33**, L01810, doi: 10.1029/2005GL024406.

Mitchell, J. F. B. and W. J. Ingram, 1992: Carbon dioxide and climate: Mechanisms of changes in cloud. *J. Clim.*, **5**, 5–21.

Pierrehumbert, R. T. and R. Roca, 1998: Evidence for control of Atlantic subtropical humidity by large scale advection. *Geophys. Res. Lett.*, **25**, 4537–4540.

Prather, M. J., 1986: Numerical advection by conservation of second-order moments. *J. Geophys. Res.*, **91**, 6671–6680.

Price, J. and R. Wood, 2002: Comparison of probability density functions for total specific humidity and saturation deficit humidity, and consequences for cloud parametrization. *Quart. J. Roy. Meteor. Soc.*, **128**, 2059–2072.

Randall, D. A., et al., 2007: Climate models and their evaluation. *Climate Change 2007: The Physical Science Basis. Contribution of Working Group I to the Fourth Assessment Report of the Intergovernmental Panel on Climate Change*, S. Solomon, D. Qin, M. Manning, Z. Chen, M. Marquis, K. B. Averyt, M. Tignor, and H. L. Miller, Eds., Cambridge University Press, Cambridge, UK and New York, NY, USA, 589–662.

Rasch, P. J., B. Boville, and G. Brasseur, 1995: A three-dimensional general circulation model with coupled chemistry for the middle atmosphere. *J. Geophys. Res.*, **100**, 9041–9072.

Rasch, P. J. and J. Kristjansson, 1998: A comparison of the CCM3 model climate using diagnosed and predicted condensate parameterizations. *J. Clim.*, **11**, 1587–1614.

Rasch, P. J., N. M. Mahowald, and B. Eaton, 1997: Representations of transport, convection, and the hydrologic cycle in chemical transport models: Implications for the modeling of short-lived and soluble species. *J. Geophys. Res.*, **102 (D23)**, 28,127–28,138.

Rasch, P. J. and D. Williamson, 1990: Computational aspects of moisture transport in global models of the atmosphere. *Quart. J. Roy. Meteor. Soc.*, **116**, 1071–1090.

Santer, B. J., et al., 2003: Contributions of anthropogenic and natural forcing to recent tropopause height changes. *Science*, **301**, 479–483.

Schmidt, G. A., et al., 2006: Present-day atmospheric simulations using GISS ModelE: Comparison to in situ, satellite, and reanalysis data. *J. Clim.*, **19**, 153–192, doi:10.1175/JCLI3612.1.

Schneider, T., P. A. O'Gorman, and X. Levine, 2009: Water vapor and the dynamics of climate changes. *Rev. Geophys.*, submitted.

Seidel, D. J. and W. J. Randel, 2006: Variability and trends in the global tropopause estimated from radiosonde data. *J. Geophys. Res.*, **111**, D21101, doi:doi:10.1029/2006JD007363.

Sherwood, S. C., 1996: Maintenance of the free-tropospheric tropical water vapor distribution. part ii: Simulation by large-scale advection. *J. Clim.*, **9**, 2919–2934.

Sherwood, S. C., W. Ingram, Y. Tsushima, M. Satoh, M. Roberts, P. L. Vidale, and P. A. O'Gorman, 2009: Relative humidity changes in a warmer climate. *J. Geophys. Res.*, submitted.

Sherwood, S. C. and C. L. Meyer, 2006: The general circulation and robust relative humidity. *J. Clim.*, **19**, 6278–6290.

Soden, B. J. and I. M. Held, 2006: An assessment of climate feedbacks in coupled ocean-atmosphere models. *J. Clim.*, **19**, 3354–3360.

Soden, B. J., R. T. Wetherald, G. L. Stenchikov, and A. Robock, 2002: Global cooling after the eruption of Mount Pinatubo: A test of climate feedback by water vapor. *Science*, **296**, 727–730.

Son, S.-W., et al., 2008: Impact of stratospheric ozone recovery on the Southern Hemisphere westerly jet. *Science*, **320**, 1486–1489.

Son, S.-W., et al., 2009: The impact of stratospheric ozone recovery on tropopause height trends. *J. Clim.*, **22**, 429–445.

Sundqvist, H., 1978: A parameterization scheme for nonconvective condensation including prediction of cloud water content. *Quart. J. Roy. Meteor. Soc.*, **104**, 677–690.

Vecchi, G. A. and B. J. Soden, 2007: Global warming and the weakening of the tropical circulation. *J. Clim.*, **20**, 4316–4340.

Waliser, D. E., et al., 2009: Influence of condensate evaporation on water vapor and its stable isotopes in a GCM. *J. Geophys. Res.*, **114**, D00A21, doi:10.1029/2008JD010015.

World Meteorological Organization, 1957: Meteorology — A three-dimensional science: Second session of the commission for aerology. *WMO Bull.*, **IV**, 134–138.

Wright, J. S., R. Fu, and A. J. Heymsfield, 2009a: A statistical analysis of the influence of deep convection on water vapor variability in the tropical upper troposphere. *Atm. Chem. Phys.*, **9**, 5847–5865.

Wright, J. S., A. H. Sobel, and G. A. Schmidt, 2009b: Influence of condensate evaporation on water vapor and its stable isotopes in a GCM. *Geophys. Res. Lett.*, **36**, L12804, doi:10.1029/2009GL038091.

Zhang, G. and N. McFarlane, 1995: Sensitivity of climate simulations to the parameterization of cumulus convection in the Canadian Climate Centre general circulation model. *Atmos.-Ocean*, **33**, 407–446.

List of Figures

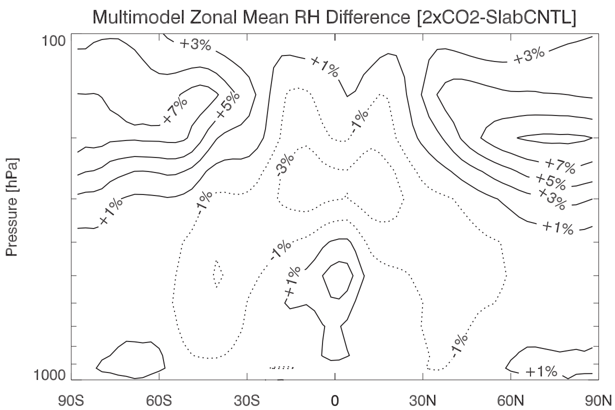

FIG. 1. Zonal mean changes in RH averaged over ten different slab ocean GCMs. Dotted contours represent decreases in the $2\times CO_2$ runs as compared to the control runs. Contour intervals are 2% RH; the first dashed contour represents a 1% absolute decrease in RH and the first solid contour represents a 1% absolute increase in RH.

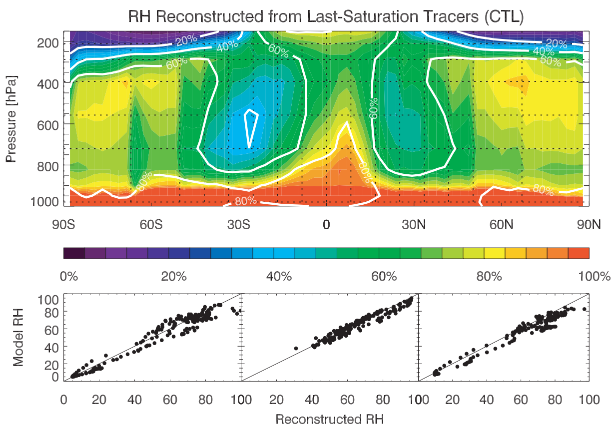

FIG. 2. Zonal mean relative humidity reconstructed from last saturation tracers for the CTL run, overplotted with RH as calculated by the MATCH internal hydrologic cycle (white contours; contour interval is 20% RH). Dashed black lines show the distribution of tracer domains. Bottom panels show a point-by-point comparison between the two modeled and reconstructed relative humidities for the latitude bands matching the abscissa above. Left to right, these regions correspond to 90°S to 30°S, 30°S to 30°N, and 30°N to 90°N.

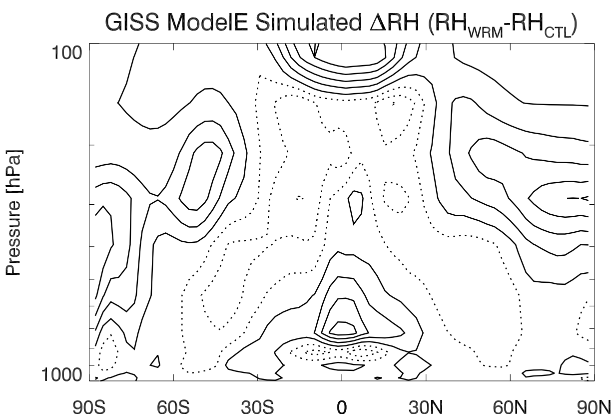

Fig. 3. Changes in zonal mean RH between the WRM and CTL runs of the GISS ModelE. Contour intervals are as in Fig. 1

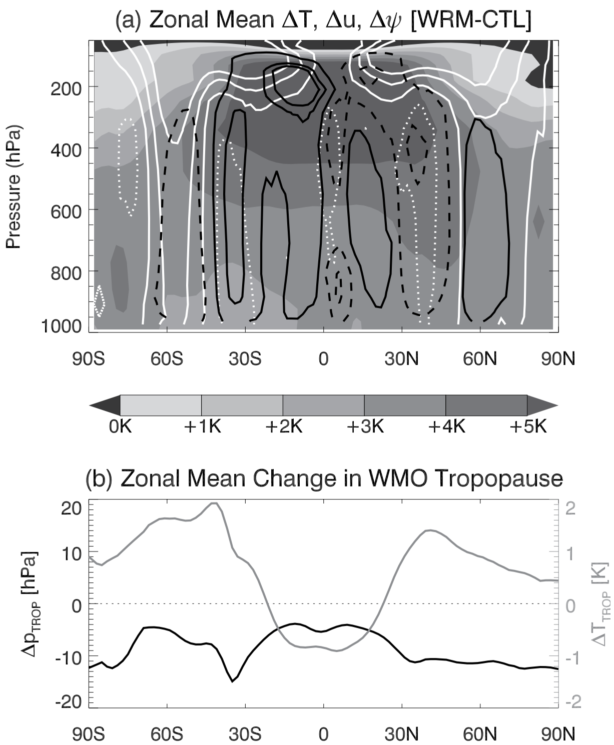

FIG. 4. (a) Annual mean zonal mean changes in simulated temperature and circulation. Shading shows temperature with a contour interval of 1 K; white contours show zonal wind with a contour interval of $1\,\mathrm{m\,s^{-1}}$, with dotted contours representing decreases; black contours show stream function with a contour interval of $4{\times}10^9\,\mathrm{kg\,s^{-1}}$, dashed contours represent decreases. (b) Annual mean zonal mean changes in the pressure and temperature of the WMO tropopause.

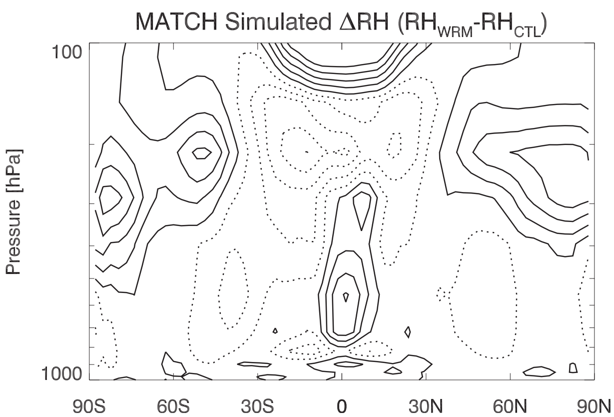

FIG. 5. Zonal mean changes in RH determined by the MATCH internal hydrologic cycle using prescribed temperatures and circulation from the GCM simulations. Contour intervals are as in Fig. 1.

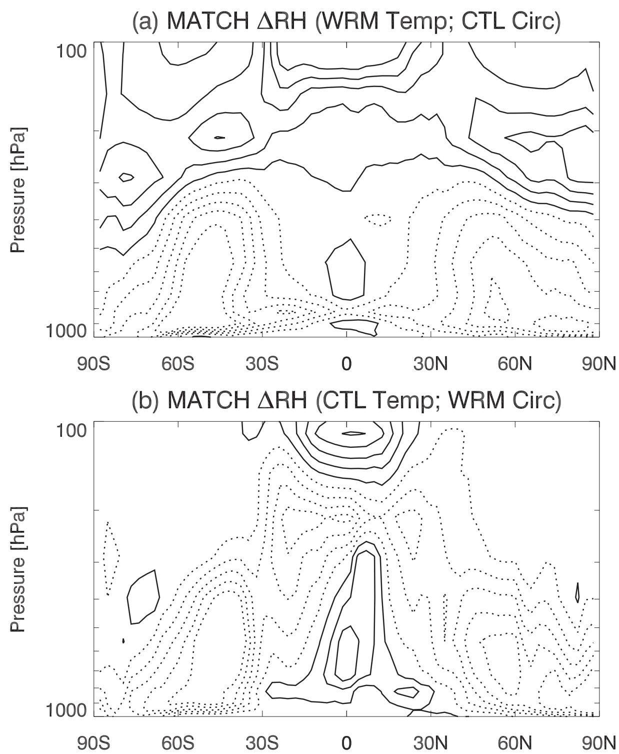

Fig. 6. Zonal mean relative humidity changes in the MATCH hydrologic cycle for (a) a run in which the input files contain WRM temperatures and CTL dynamics and (b) a run in which the input files contain WRM dynamics and CTL temperatures. Contour intervals are as in Fig. 1.

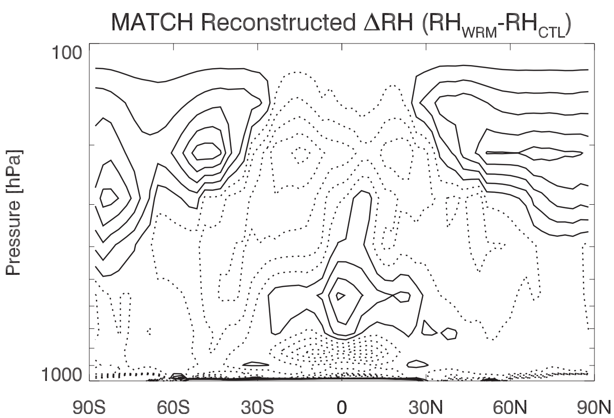

FIG. 7. Annual mean zonal mean changes in relative humidity reconstructed from the last saturation tracers. Contour intervals are as in Fig. 1.

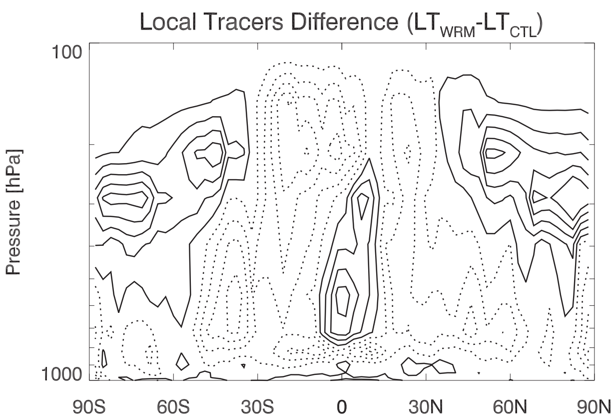

FIG. 8. Annual mean zonal mean changes in local tracer concentration. Contour intervals are 2%; the first dashed contour represents a 1% absolute decrease and the first solid contour represents a 1% absolute increase.

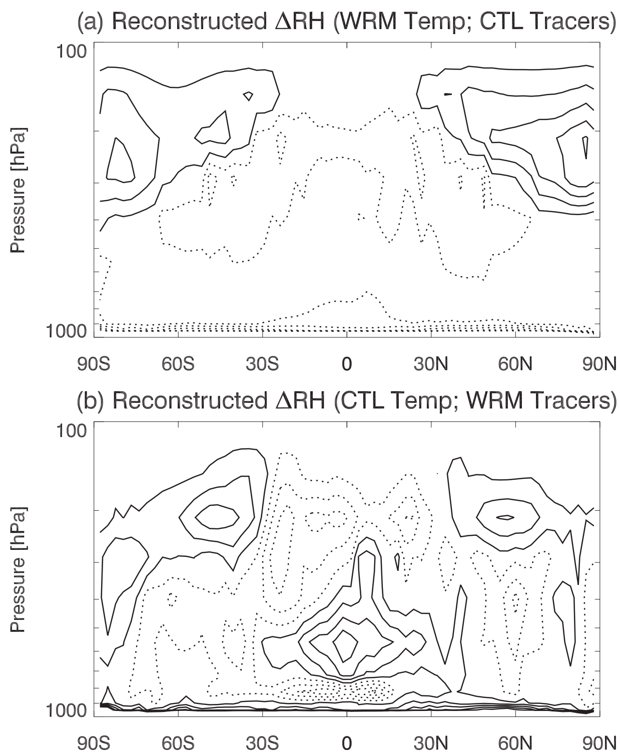

FIG. 9. Zonal mean changes in RH reconstructed from the last saturation tracers using (a) WRM temperatures and CTL tracers and (b) WRM tracers and CTL temperatures. Contour intervals are as in Fig. 1

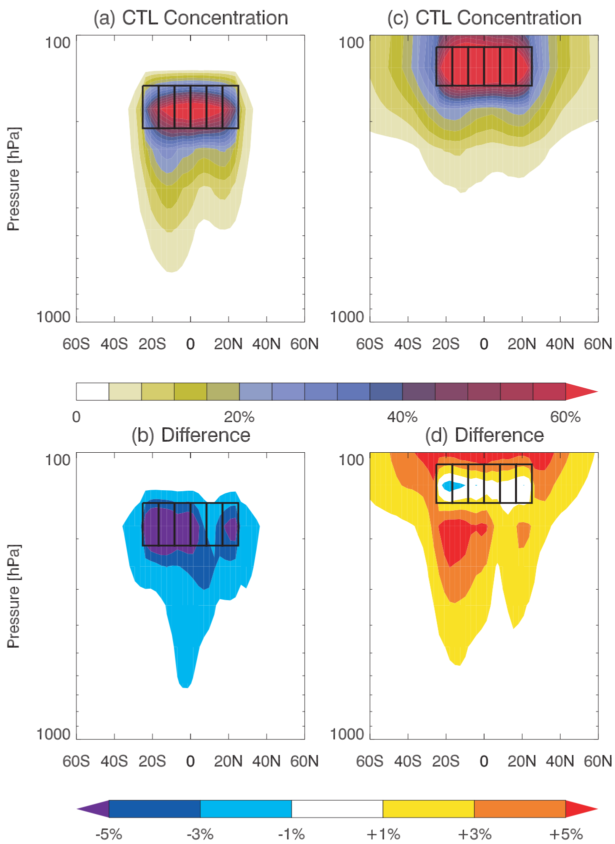

Fig. 10. Shifts in last saturation tracer concentrations in the tropical upper troposphere. The left panels show (a) the distribution of tracers associated with the 288 hPa to 212 hPa layer between approximately 25°S and 25°N for the CTL MATCH simulation, and (b) the difference between the distributions of these tracers in the WRM and CTL simulations. The right panels show the same quantities for tracers associated with the same latitude range but for the 212 hPa to 150 hPa pressure layer.

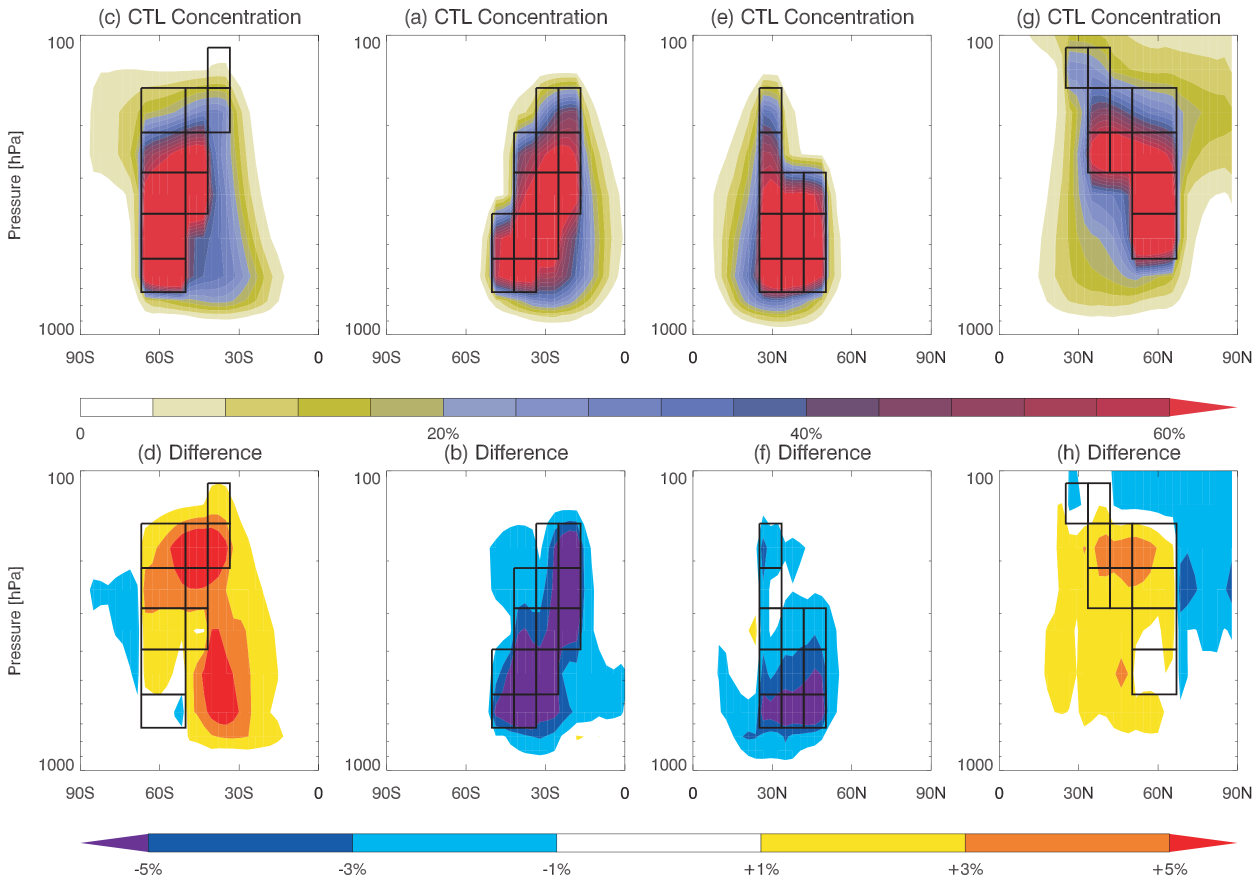

FIG. 11. Shifts in last saturation tracer concentrations in the northern hemisphere subtropics and extratropics. As in Fig. 10 but for tracers controlling humidity in the (a)-(d) Southern Hemisphere subtropics and (e)-(h) Northern Hemisphere subtropics.